General Disclaimer

One or more of the Following Statements may affect this Document

- This document has been reproduced from the best copy furnished by the organizational source. It is being released in the interest of making available as much information as possible.

- This document may contain data, which exceeds the sheet parameters. It was furnished in this condition by the organizational source and is the best copy available.

- This document may contain tone-on-tone or color graphs, charts and/or pictures, which have been reproduced in black and white.

- This document is paginated as submitted by the original source.

- Portions of this document are not fully legible due to the historical nature of some of the material. However, it is the best reproduction available from the original submission.

PNL-4259
UC-48

Develop Real-Time Dosimetry Concepts and Instrumentation for Long-Term Missions

Technical Progress
February 1981 to February 1982

L. A. Braby

May 1982

Prepared for
National Aeronautics and Space Administration
Lyndon B. Johnson Space Center
under a Related Services Agreement
with the U.S. Department of Energy

PNL-4259

Pacific Northwest Laboratory
Operated for the U.S. Department of Energy
by Battelle Memorial Institute

Battelle

PNL-4259
UC-48

DEVELOP REAL-TIME DOSIMETRY CONCEPTS AND INSTRUMENTATION FOR LONG-TERM MISSIONS

Technical Progress
February 1981 to February 1982

L.A. Braby

May 1982

Prepared for
National Aeronautics and Space Administration
Lyndon B. Johnson Space Center
Order No. T-794H
under a Related Services Agreement
with the U.S. Department of Energy
under Contract DE-AC06-76RLO 1830

Pacific Northwest Laboratory
Richland, Washington 99352

CONTENTS

FIGURES iii

TABLES iii

INTRODUCTION 1

DETECTOR DEVELOPMENT 1

ELECTRONIC SYSTEM 2

EVALUATION OF RADIATION QUALITY 6

FUTURE DIRECTION 15

REFERENCES 16

FIGURES

1. Detector Gas Gain at a Constant Anode Voltage as a Function of Time After Sealing the Detector 2
2. Gas Gain Versus Anode Voltage 3
3. Flow Diagram of the Subroutine and Block Diagram of Hardware for Adjusting the Anode Voltage to Maintain Constant Gas Gain . 4
4. Block Diagram of a System Using Two Detectors to Cover a Wide Range of Event Sizes 5
5. Detailed Block Diagram of the Electronics for the High Gain Detector 6
6. Analog to Digital Converter Using CMOS Successive Approximation Circuit 7
7. Prototype Portable Instrument with the High Gain Detector . . 8
8. Typical Curves for the Density of Dose in Lineal Energy for Neutron and Mixed Field Irradiations 11
9. Mean and Standard Deviation for Forty Repetitions of $\overline{Q} = 0.8 + 0.14\ \overline{y}_D$ at Each Value of the Dose 12
10. Mean and Standard Deviation for 40 Samples of $\overline{Q}$ Determined by a Fourier Transform Deconvolution of the LET Distribution at Each Dose 13

TABLES

1. Power Consumption 8
2. Mean Value for 40 Calculations of Quality 13
4. Milestones 15

DEVELOP REAL-TIME DOSIMETRY CONCEPTS AND INSTRUMENTATION FOR LONG TERM MISSIONS

INTRODUCTION

Major objectives in the process of developing a rugged portable instrument to evaluate dose and dose equivalent have been achieved. A tissue-equivalent proportional counter simulating a 2 micrometer spherical tissue volume has operated satisfactorily for over a year. The basic elements of the electronic system have been designed and tested. And finally, the most suitable mathematical technique for evaluating dose equivalent with a portable instrument has been selected. Design and fabrication of a portable prototype, based on the previously tested circuits, is underway.

DETECTOR DEVELOPMENT

The 5.7 cm detector has been operated for over 15 months with the original gas filling. Figure 1 shows the gas gain for a constant anode voltage during that time. The long-term drift, less than one percent per month, and short-term (less than 24 hour) variations of ± 2 percent can easily be controlled by adjusting the anode voltage, (see Figure 2). These adjustments will be made automatically by a subroutine, illustrated in Figure 3, which compares the actual position of a calibration peak with the position of that peak at the proper gas gain. The difference is used to calculate a new high-voltage supply setting. The actual voltage is provided by a high-voltage supply referenced to the output of a digital-to-analog converter.

The detector will be operated with a combination of gas gain and electronic gain which results in a calibration factor of 0.12 keV/μm/channel and a useful range of 0.36 to 300 keV/μm. Since the dose mean of the single-event distribution for X and γ rays varies from 0.7 to 3.0 keV/μm, and for neutrons from 30 to 130 keV/μm, the system is expected to detect photon as well as neutron dose. However, the stainless steel vacuum chamber surrounding the detector will distort the response as a function of photon energy. Also, the photon-induced events cannot be distinguished from very low-energy neutron events.

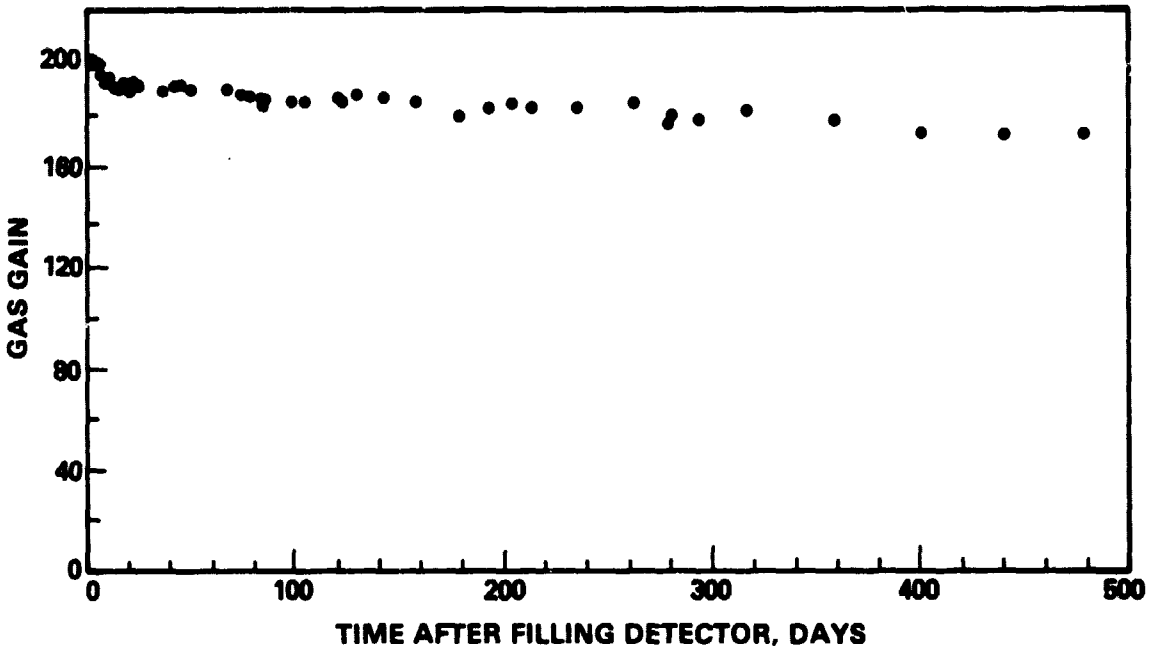

FIGURE 1. Detector Gas Gain at A Constant Anode Voltage as a Function of Time After Sealing the Detector

Thus, though the system is expected to accurately measure dose due to photons and low-energy neutrons, estimates of the mean quality factor become less certain when low-energy neutrons are abundant.

Specifications for the second detector, intended to detect high-energy heavy particles, have been completed. It will use the same basic design and materials but will be 12.7 cm in diameter in order to provide approximately five times the counting rate.

ELECTRONIC SYSTEM

The electronics for a system using two detectors is outlined in Figure 4. Each detector is supported by a dedicated high-voltage supply, amplifiers and analog-to-digital converters (ADC's), but the two detectors share a multichannel analyzer (MCA) and microcomputer. The ADC's output is used as a MCA memory address. Each event results in a "one" being added to the memory content at

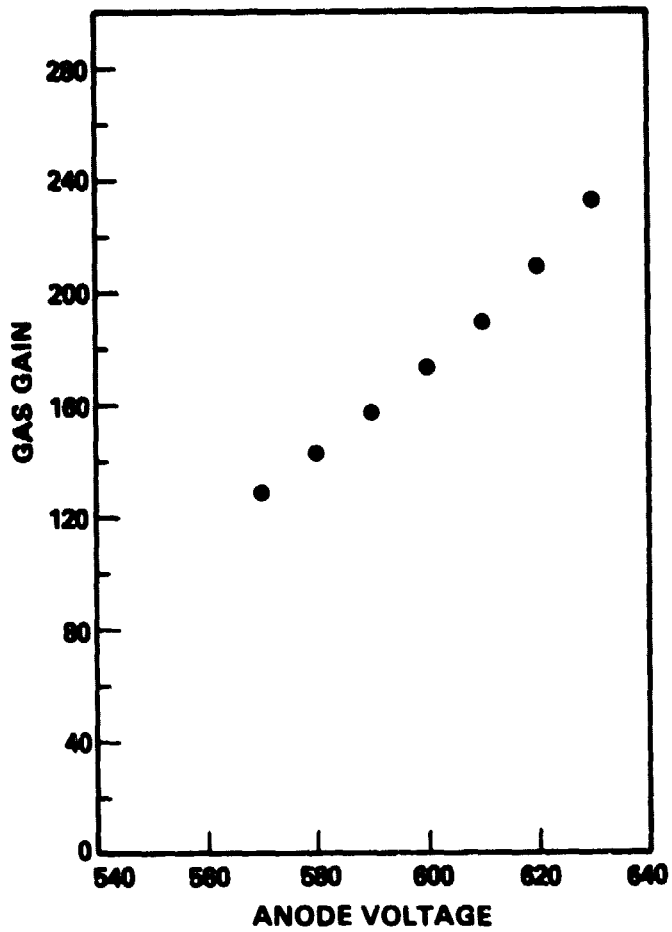

FIGURE 2. Gas Gain Versus Anode Voltage

the corresponding address. As illustrated in Figure 5, the entire MCA content can be periodically transferred to the microcomputer memory. The dosimetric quantities can then be computed without interrupting further data collection. An absolute time clock in the microcomputer is used to initiate the dose calculation, data storage, calibration and other functions. A CMOS successive approximation ADC chip and other CMOS components are used in the ADC circuit, in Figure 6, to minimize power consumption.

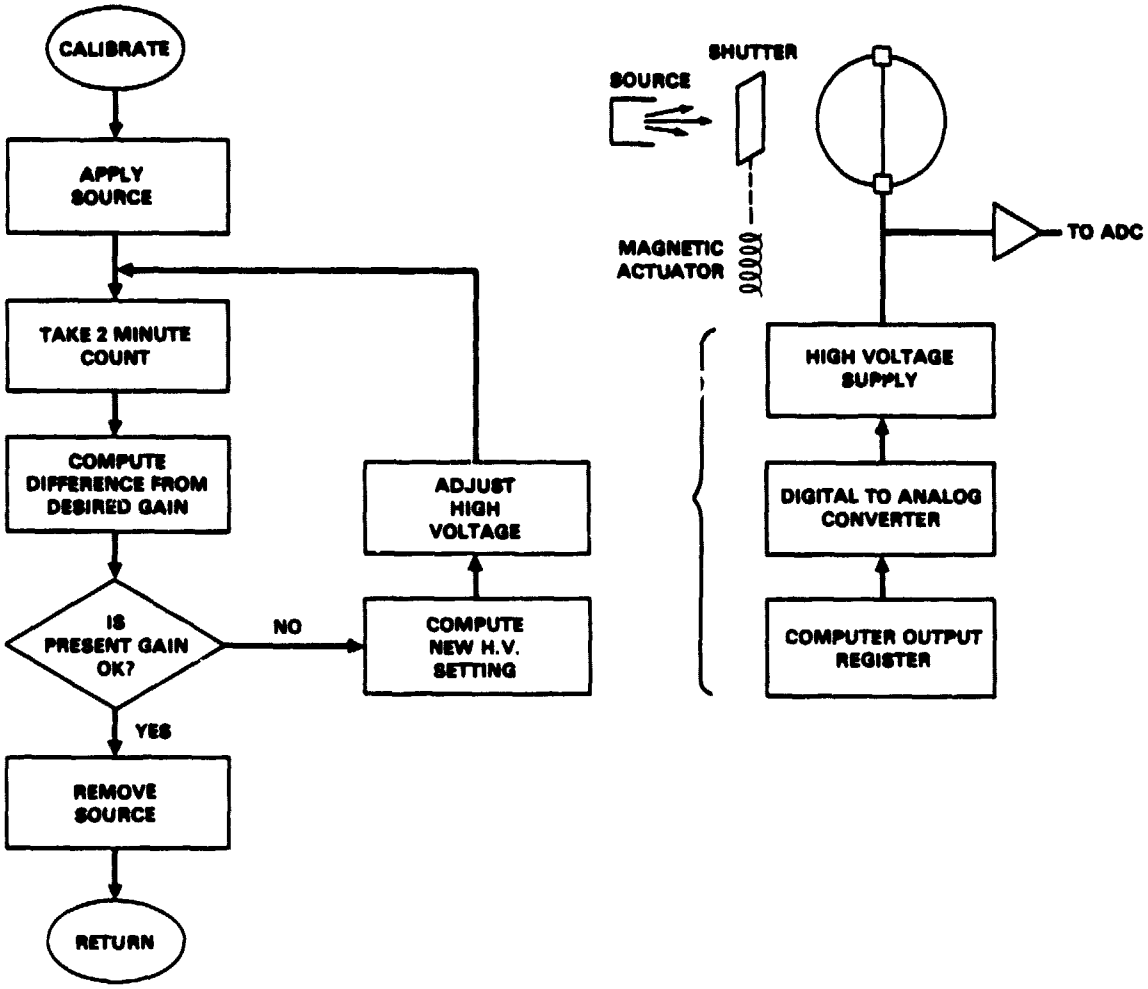

FIGURE 3. Flow Diagram of the Subroutine and Block Diagram of Hardware for Adjusting the Anode Voltage to Maintain Constant Gas Gain

Preliminary versions of all of this circuitry have been assembled and are being tested in the laboratory prototype described previously (PNL-3747, Braby 1981). Power consumption, an important feature in a portable system, is listed in Table 1 for the current versions of the main components. These designs have established the physical and electronic requirements for a prototype portable instrument. Mechanical work on this portable prototype (see Figure 7) has been

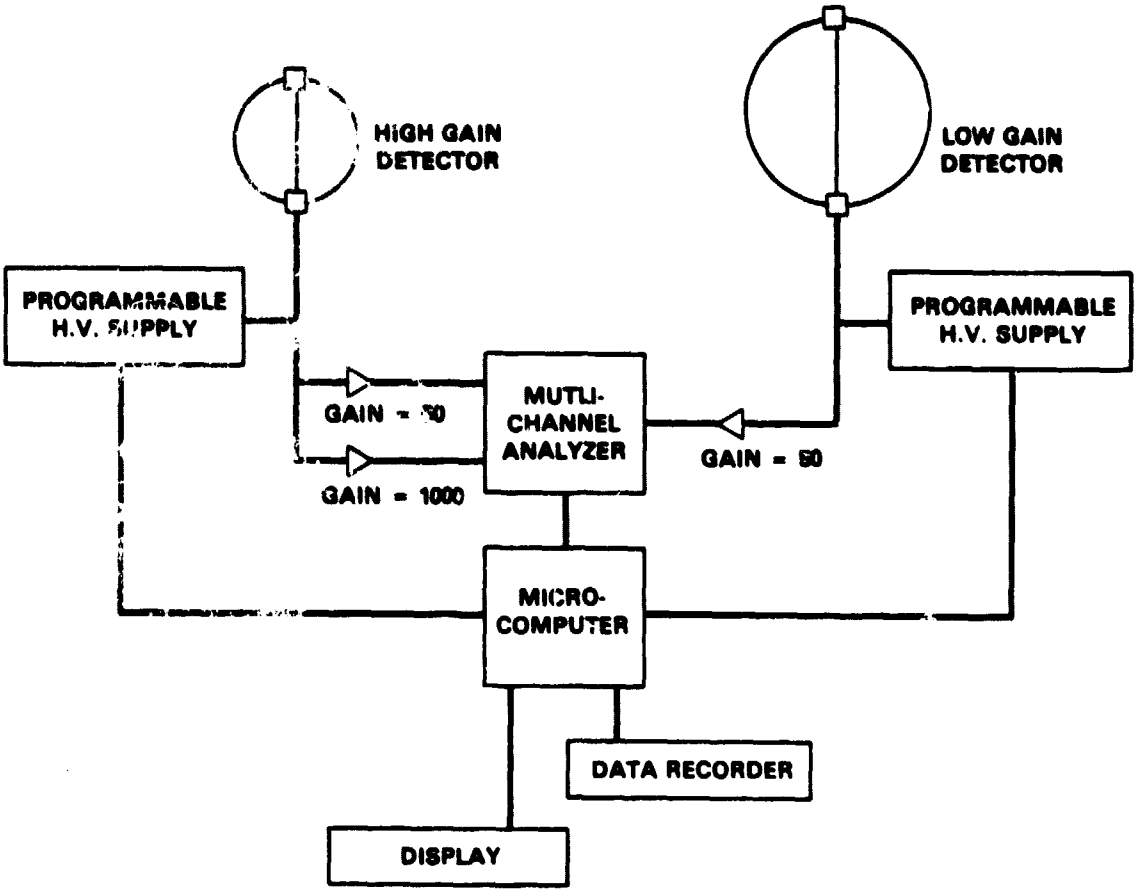

FIGURE 4. Block Diagram of a System Using Two Detectors to Cover a Wide Range of Event Sizes

completed. As individual circuits are refined and power consumption is reduced, cards will be assembled for use in this prototype. For convenience in making calibration measurements, it has been equipped with operator controls such as acquire, reset, and record. These functions will be controlled by the microcomputer when the system is complete. During testing, the operating program will be in random access memory and can be easily altered and re-entered via an RS232 port. For routine operation, the same program will be installed in a read-only memory to avoid having to re-enter the program after a power loss.

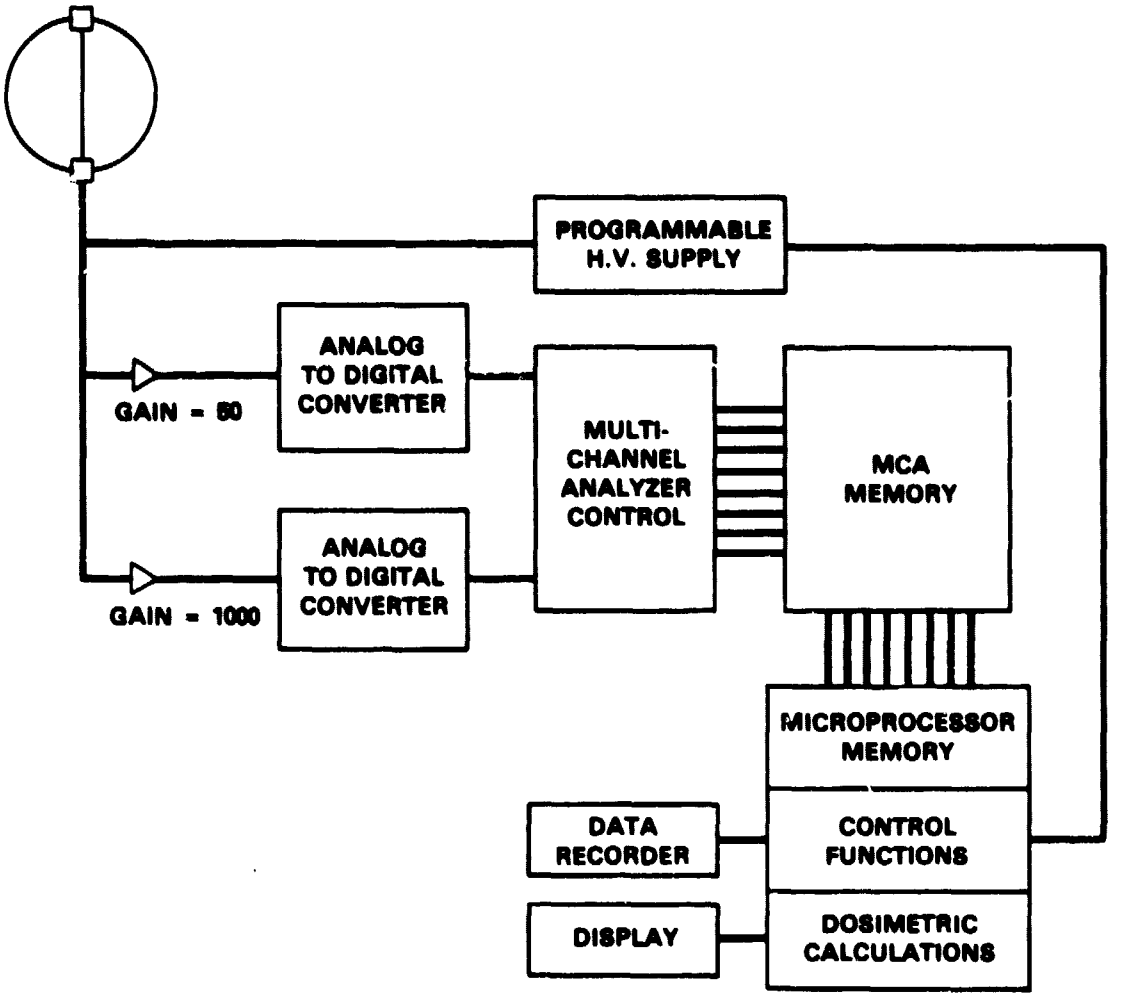

FIGURE 5. Detailed Block Diagram of the Elec-
ronics for the High-Gain Detector

EVALUATION OF RADIATION QUALITY

There are two basic ways of determining the quality factor based on the measured probability density of energy imparted, $f(\varepsilon)$, or related functions such as $f(y)$, the density of y where y is related to the mean cord length $\bar{l}$ by $y = \varepsilon/\bar{l}$, and the density of dose in y, $d(y) = yF(y)$. The first method involves direct application of the lineal energy, usually in the form of $d(y)$, and the second method involves the deconvolution of the LET distribution from

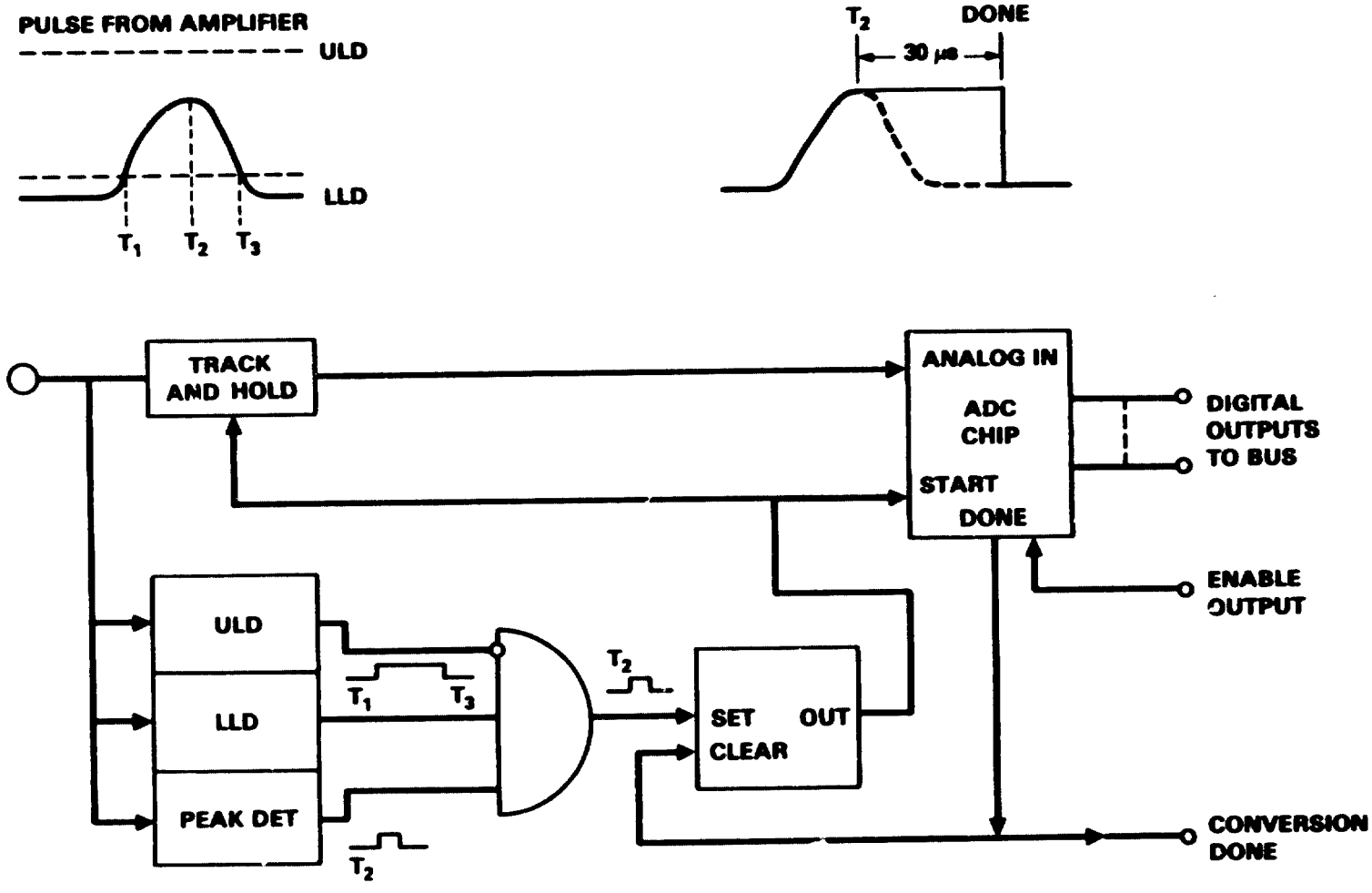

FIGURE 6. Analog to Digital Converter Using CMOS Successive Approximation Circuit

TABLE 1. Power Consumption

Circuit	Power Watts	Number Required in Two-Detector System	Total Watts
preamp	0.2	2	0.4
amplifier	1.1	2	2.2
H.V. supply	1.6	2	3.2
A.D.C.	0.75	3	2.25
MCA	0.05	1	0.05
microcomputer	0.35	1	0.35
memory	∿0.2	1	0.2
display	∿0.1	1	0.1
tape recorder	1	∿5% duty cycle	0.05
			8.80

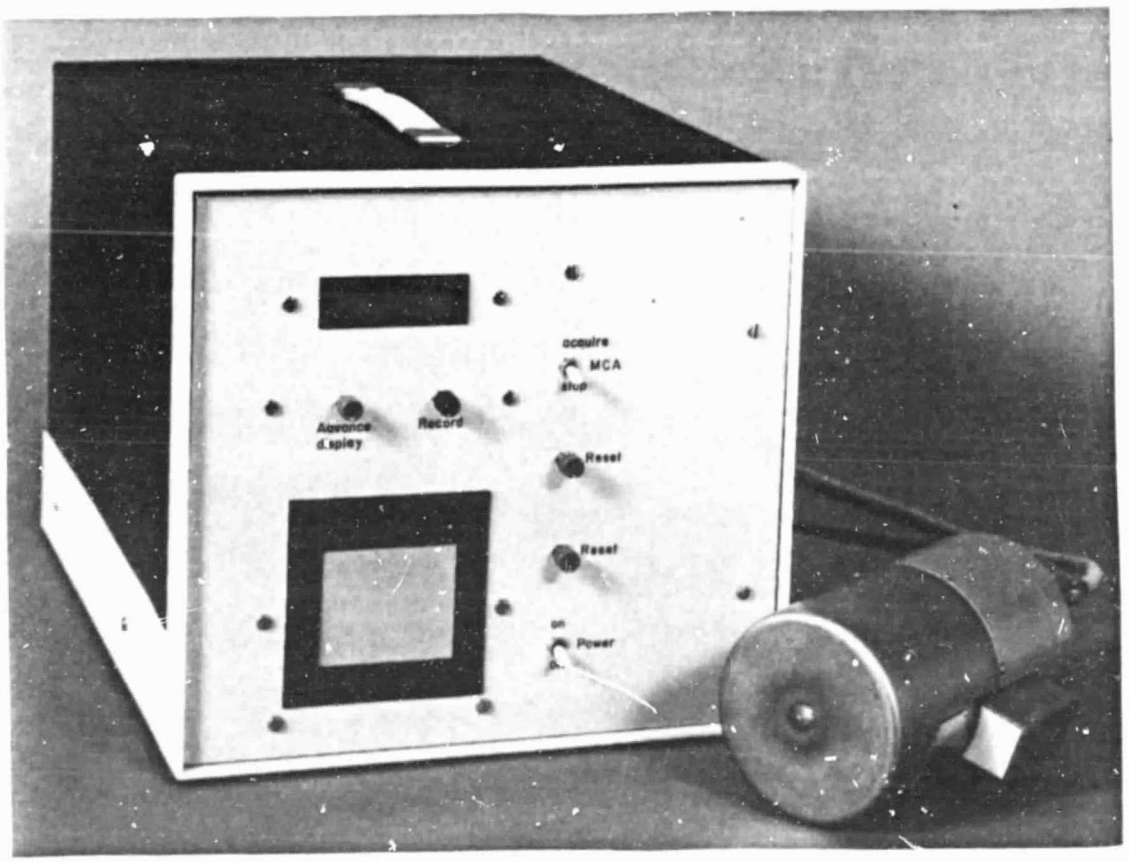

FIGURE 7. Prototype Portable Instrument with the High Gain-Detector

the y distribution (see for example Rossi, 1968). If one assumes that energy-loss straggling and delta-ray effects are insignificant and that all of the tracks are long compared to the site diameter so that there is no stopping or starting within the detector volume (Kellerer 1969) and if one further assumes a functional form for the relationship between LET and quality factor, one can derive

$$Q = 0.8 + 0.14\ \bar{y}_D \tag{1}$$

where $\bar{y}_D$ is the dose mean of the lineal energy.

A second way of applying y directly,

$$Q = \int_0^\infty y^{*1.5}\, d(y)dy, \tag{2}$$

was proposed by Rossi (1977) as a new definition for quality factor. The quantity y* is a saturated version of the lineal energy intended to take into account the fact that RBE generally decreases for LET values above about 150 keV/μ. This formulation of Equation 2 was intended to provide very large values of the radiation quality, in line with biophysics models which suggest that the quality factor should be 10 to 20 times higher than the current definition. However, this same method can be applied to give quality factors in line with current definitions by substituting 0.6 for the exponent 1.5 in Equation 2.

The simplest of the methods for unfolding LET distribution from the single-event distribution measured in the spherical detector is

$$d(L_\infty) = \frac{L_\infty d}{2}\left(f(\epsilon) - \epsilon\frac{df(\epsilon)}{d\epsilon}\right) \tag{3}$$

where $d(L_\infty)$ is the density of absorbed dose in LET,[a] d is the site diameter, and $f(\epsilon)$ is the density of energy imparted. This method is based on the fact

(a) In ICRU 19 and 33 the symbol D_{L_∞} is used for $d(L_\infty)$

that a spherical detector produces a triangular cord-length distribution and the contribution of any given LET to the overall distribution can be found from the slope of the distribution for energy imparted corresponding to that value of LET. Once the dose distribution in LET has been derived, the definition for the mean quality factor given in ICRU 19 and 33 is;

$$\overline{Q} = \int_0^\infty Q\, d(L_\infty)\, dL_\infty \Big/ \int_0^\infty d(L_\infty) dL_\infty \qquad (4)$$

and can be utilized to get the mean quality factor.

Another method for unfolding the dose distribution of LET was proposed by Kellerer (1972). This involves generating the Fourier transform of both the distribution of energy imparted and the track-length distribution. The quotient of these two is the transform of the LET distribution. The reverse transform provides the desired distribution, $d(L_\infty)$. While this process sounds complicated, algorithms for the fast Fourier transform are available even for small microprocesser-based computers and this unfolding technique can easily be applied in a microcomputer with 8K bytes of memory.

Each of these methods was tested using simulated spectra corresponding to specified doses. A smooth distribution for a specific neutron energy, derived from the literature, was entered as data. Random number generators were then used to generate a simulated measurement with the appropriate statistical variation for the specified dose. The algorithm being tested was used to calculate the quality factor for that simulated distribution and the result was stored. Then a new distribution for the same dose and initial distribution was generated and another value of the quality factor was calculated. This procedure was repeated 40 times for each dose. Finally a mean and standard deviation of the quality factor for those 40 simulated measurements was calculated.

All of the methods of calculating quality involved the dose distribution either of y or LET. That is, they involved the frequency of events multiplied by the event size. This adds substantial weight to high values of y or LET so that, even though there are relatively few events at the high values of y, these

values have a large effect on the estimate of the quality. Figure 8 gives several microdosimeter distributions for neutrons and mixed fields in terms of yd(y) plotted versus the log of y so that equal areas under the curve represent equal doses. These smoothed curves were used as the starting point for calculations of the distributions to be expected from experimental measurements at various dose levels.

Figure 9 shows the mean and standard deviation of $\bar{Q}$ determined by the method in Equation 1 (Equation 2 results in similar lines but with smaller standard deviations). The value of $\bar{Q}$ is constant for each radiation as a function of dose, but the standard deviation for the estimate of $\bar{Q}$ increases rapidly from less than a percent at 10^{-2} rads to over 9 percent at 10^{-5} rads for the

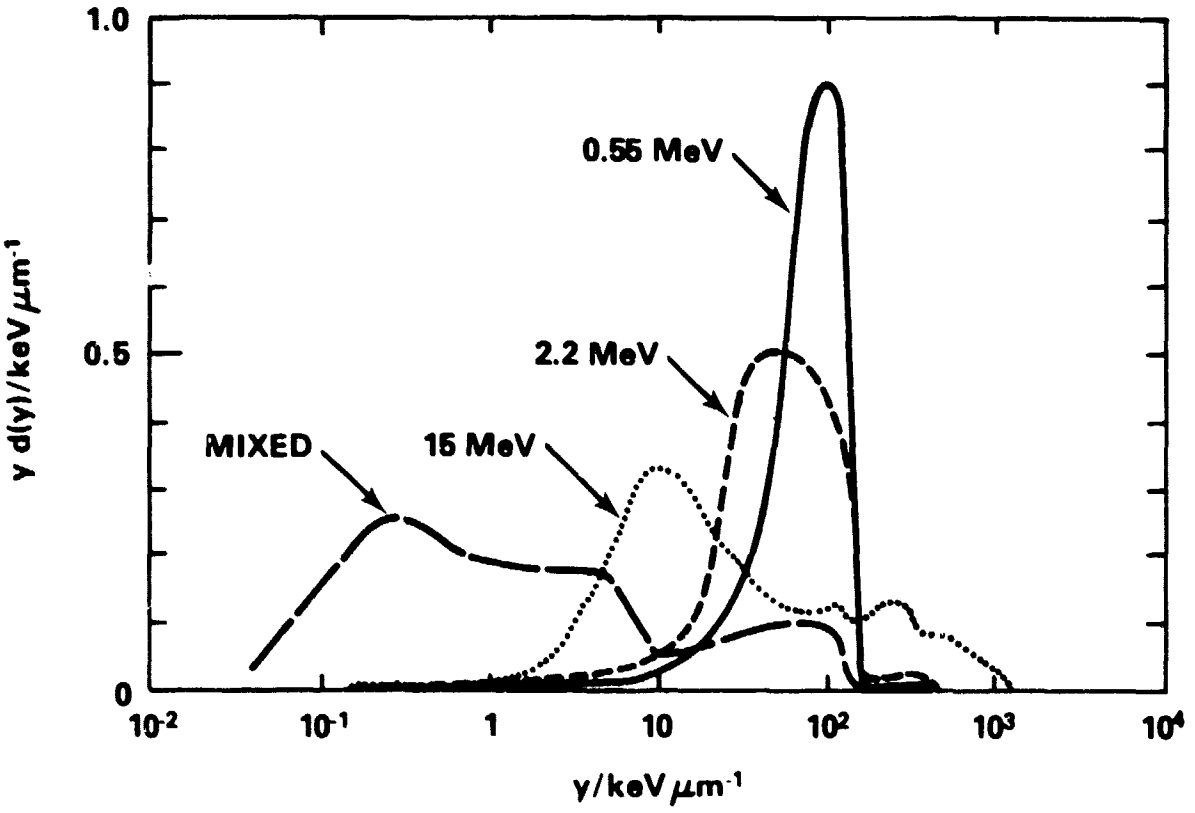

FIGURE 8. Typical Curves for the Density of Dose in Lineal Energy for Neutron and Mixed Field Irradiations

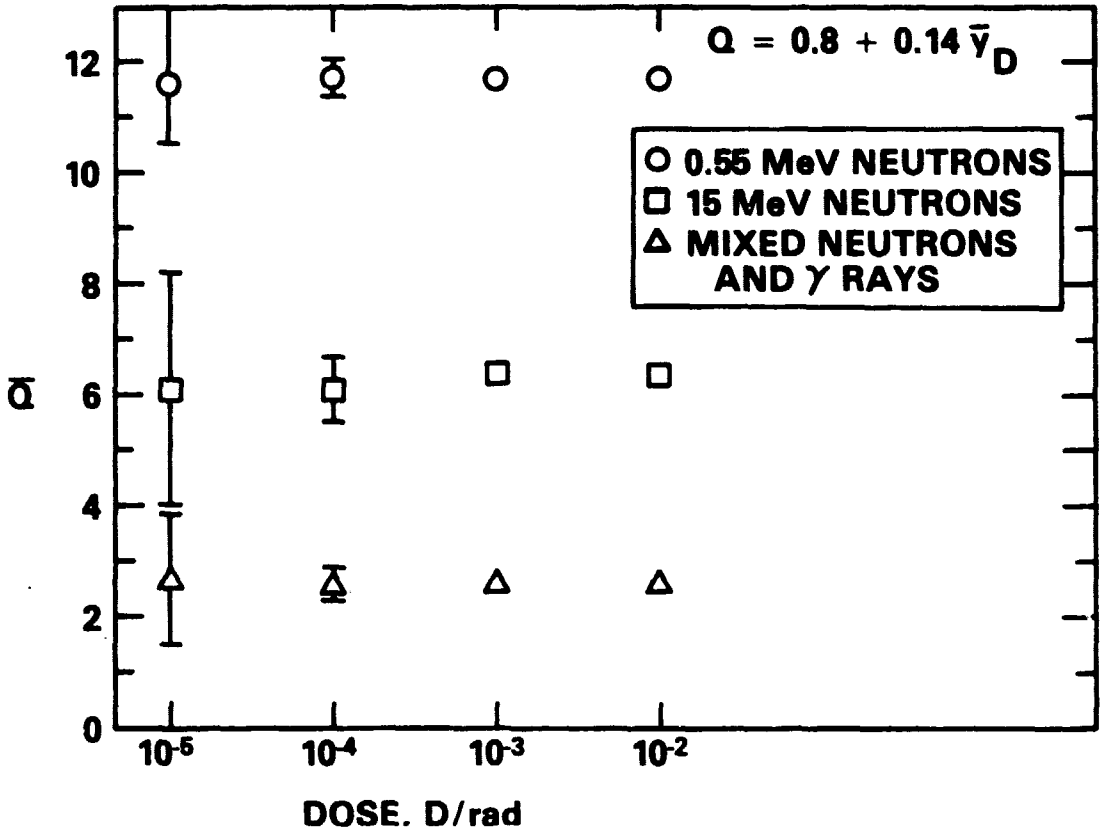

FIGURE 9. Mean and Standard Deviation for 40 Repetitions of $\bar{Q} = 0.8 + 0.14\ \bar{y}_D$ at Each Value of the Dose

half MeV neutrons. Figure 10 is the equivalent result using the Fourier transform method. This has the unfortunate nature that as the dose decreases, the mean of the 40 samples of $\bar{Q}$ decreases abruptly, and the standard deviation increases rapidly. In fact it is not possible to get an estimate of $\bar{Q}$ at 10^{-5} rads for the 15 MeV neutrons or even at 10^{-4} rads with a mixed-neutron gamma ray field. This is due to high-frequency components in the transform resulting from the noise in $F(\varepsilon)$. These high-frequency components lead to negative values for the density of LET.

Table 2 gives the mean value for 40 calculations of quality as defined by Equations 1 through 4 for each of the y distributions illustrated in Figure 8 at the dose of 10^{-2} rads, and also gives the ICRP report 21 maximum

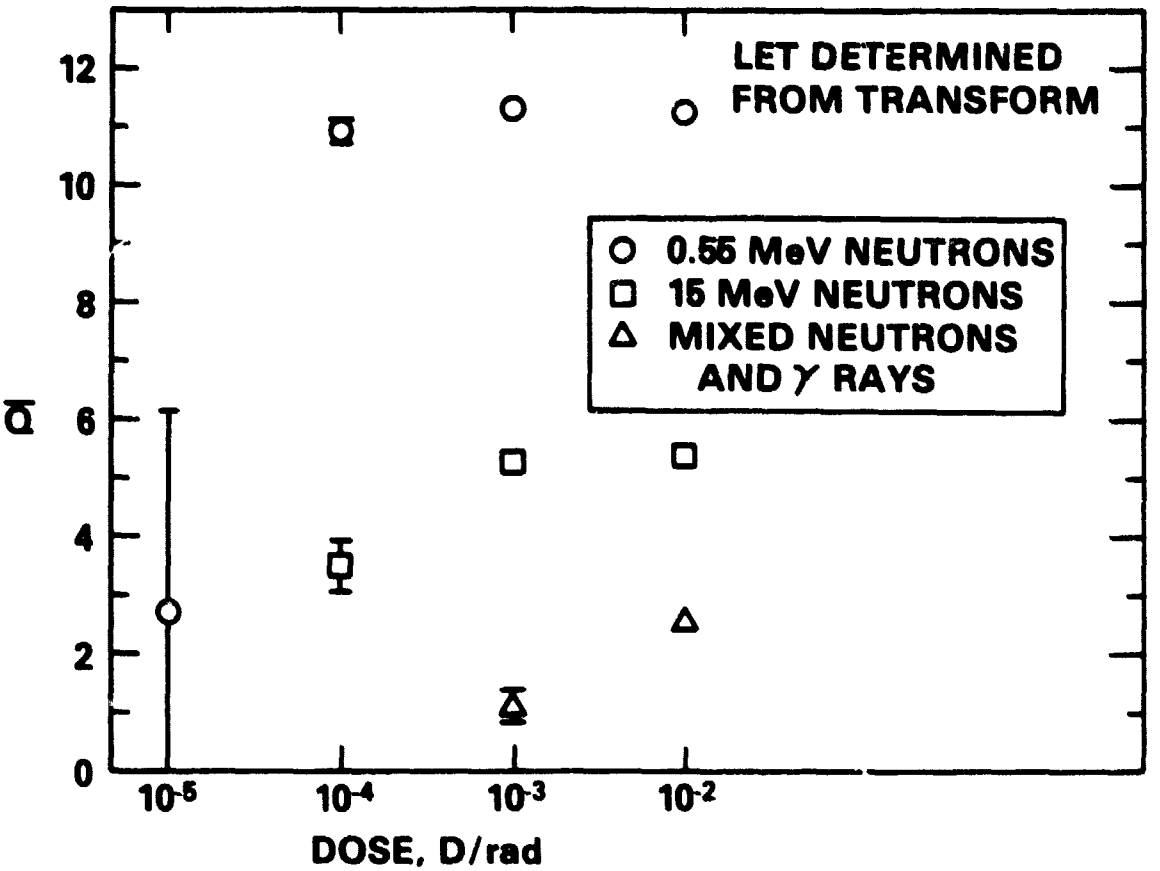

FIGURE 10. Mean and Standard Deviation for 40 Samples of $\bar{Q}$ Determined by a Fourier Transform Deconvolution of the LET Distribution at Each Dose

TABLE 2. Mean Value for 40 Calculations of Quality

Equations	Mixed Field	0.55 MeV	2.2 MeV	15 MeV
1) $\bar{Q}_a$	2.6	11.7	12.5	6.4
2) $\bar{Q}_b y^{*1.5}$	69.3	476	461	184
$y^{*0.6}$	2.9	10.9	11.2	6.6
3) $\bar{Q}_c$	4.7	13.6	16.4	9.7
numerical filtering	3.7	14.8	16.4	8.0
4) $\bar{Q}_e$	2.6	11.3	11.2	5.4
ICRP21[a]		11	9.2	6.4

(a) ICRP report maximum quality for monoenergetic neutron sources.

quality for the monoenergetic neutron sources. Since there is no direct comparison between the spectra used in these calculations and the ICRP report calculations, this cannot be taken as a good indication of the accuracy of these calculational methods, but does give a rough idea of the accuracy which might be obtained. Clearly even for 15 MeV neutrons, which should show substantial straggling, the method outlined in Equation 1 produces a surprisingly satisfactory value for the quality factor. Equation 2, using the original exponent of 1.5 is intended to produce very large values of quality and in fact does. However, substituting the exponent 0.6 this method provides equally good, if not better values of the quality than Equation 1 did. The method involving Equation 3 for the deconvolution of LET from y distribution is somewhat less successful. It tends to overestimate the quality in almost all situations. Some numerical filtering to smooth the differentiation process reduces the overestimations somewhat but does not eliminate the problem. The Fourier transform method produces values of the quality which are consistent with the methods based directly on y distributions but is less satisfactory in that it loses precision much more rapidly. Table 3 summarizes the relative standard deviation of the value of $\bar{Q}$ at a dose of 10^{-4} rads for the four equations, giving conventional values of $\bar{Q}$. This shows that the method of Equation 2 produces the least variation between measurements at low doses.

TABLE 3. Percent Relative Standard Deviation at 10^{-4} Rad

	Equations	Mixed Field	0.55 MeV	2.2 MeV	15 MeV
1)	Q_a	11.2	2.9	4.4	9.7
2)	$Q_{b(y^*0.6)}$	6.9	1.1	1.3	3.8
3)	Q_c	20.3	3.0	1.8	10.8
4)	Q_e	--	1.5	1.4	12.9

Based on these calculations for monoenergetic neutrons, it is evident that the method of Equation 2 (with the exponent set at 0.6) has several advantages over the other methods of calculating $\bar{Q}$. It is relatively simple compared to unfolding d(L), it produces mean values in agreement with the other methods and ICRP recommendations, the mean value does not decrease with dose, and the

estimates show the least variation at low doses. In addition, this method is least likely to overestimate the quality factor for very high LET particles. The method of Equation 1 would be a good second choice, its accuracy is good and it does not change significantly with dose, but the precision is significantly poorer.

FUTURE DIRECTION

All of the major components needed for the portable instrument have now been demonstrated. The portable prototype will be assembled as refinements in individual circuits are completed. This instrument will utilize the method of Equation 2 to evaluate dose equivalent, and will be tested in a variety of different radiation fields. Milestones for the next twelve months are listed in Table 4.

TABLE 4. Milestones

June 1, 1982	Complete portable prototype hardware
July 1, 1982	Complete electronic testing and initiate testing with external radiation sources
October 1, 1982	Complete initial testing with monoenergetic neutrons
November 15, 1982	Test low-gain detector with high-energy heavy particles
January 15, 1983	Install operating program in read-only memory.

NOTE: Some previous milestones were delayed approximately four months due to a period of no-cost extension of the contract.

REFERENCES

Braby, L. A. 1981. Develop Real-Time Dosimetry Concepts and Instrumentation for Long Term Missions, Technical Progress, February 1980-February 1981. PNL-3747, Pacific Northwest Laboratory, Richland, Washington.

Rossi, Harald H. 1968. "Microscopic Energy Distribution in Irradiated Matter." Radiation Dosimetry. Second Edition, Vol. 1, p. 43-92, Ed. by Frank H. Attix and William C. Roesch, Academic Press, New York, New York.

Kellerer, A. M. 1970. "Analysis of Patterns of Energy Deposition," Second Symposium on Microdosimetry, Ed. by H. G. Ebert, Commission of the European Communities, Brussels.

Rossi, Harald H. 1977. "A Proposal for Revision of the Quality Factor," Radiation and Environmental Biophysics. 14, pp. 275-283.

Kellerer, A. M. 1972. "An Algorithm for LET Analysis, Phys." Medicine and Biology, 17, pp. 232-240.